Compressibility Effects on the Aerodynamic Surface Quantities of Hypersonic Gap Flows

Luis T. L. C. Paolicchi and Wilson F. N. Santos
Combustion and Propulsion Laboratory (LCP)
National Institute for Space Research (INPE)
Cachoeira Paulista-SP, 12630-000
BRAZIL

Abstract

Numerical simulations of two-dimensional steady hypersonic flow in a gap at different length-to-depth (L/H) ratio and freestream Mach number are performed by using a Direct Simulation Monte Carlo (DSMC) method. The L/H ratio varies from 1 to 1/4 and the freestream Mach number ranges from 5 to 25. The work focuses on the effect in the aerodynamic surface quantities, such as heat transfer, pressure and skin friction coefficients due to variations in the gap L/H ratio as well as in the freestream Mach number. It was found that the aerodynamic surface quantities presented a large dependence on the L/H ratio, and a small dependence on the Mach number for the range investigated. The analysis showed that pressure and heating loads presented the maximum values along the downstream face, more precisely, at the shoulder of the gaps. Moreover, pressure and heating loads are at least twice larger than those for a smooth surface.

1. Introduction

The boundary layer developing over any hypersonic vehicle will inevitably be disturbed by discontinuities along the surface of that vehicle. These discontinuities regularly appear as cavities, forward- and backward-facing steps, or gaps, as in joints and between insulation tiles in shuttle orbiter vehicles. Small gaps between the tiles will allow for differential expansions, which result from varied thermal conditions of the exposed surface during a mission. Usually, such surface discontinuities may constitute in a potential source in a heat flux rise to the surface or even though in a premature transition from laminar to turbulent flow. In addition, they can be a significant source of additional pressure fluctuation on the body which can be manifested as radiated noise. As a result, the knowledge of the factors that affect the thermal and aerodynamic loads acting on the vehicle surface becomes imperative.

Hypersonic flow over gaps may cause locally thermal and aerodynamic loads which may dramatically exceed the ones of a smooth contour, normally assumed in the thermal and aerodynamic analysis. In order to operate safely, these loads have to be predicted correctly. This can be done either by experiments, which are often very expensive for real flight conditions, or by numerical simulations, which are getting continuously increasing importance.

There have been a considerable number of experiments and numerical simulations concerned with gap flows [1, 2, 3, 4, 5, 6, 7, 8, 9, 10, 11]. These research studies have been conducted in order to understand the physical aspects of a subsonic, supersonic or hypersonic flow past to this type of surface discontinuity. For the purpose of this introduction, it will be sufficient to describe only a few of these studies.

Scott and Maraia [2] have investigated the heating rate distribution and the temperature response on the gap walls of protection tiles. The analysis showed that the hottest location measured in the gap was at 0.75 inch from the upstream transverse gap, and the heat flux distribution in the gap was not constant in time, since the convective heating rate depended on the wall temperature of the gap. In addition, they have demonstrated that the heating rate depended on the gap width.

Hinderks et al. [9] have investigated the gap flow structure. They showed that exist a complex flow within the gap, consisting of a vortex superposed by an axial flow. The analysis showed that the heat flux transferred to the structure depends on the thermal state of the structure. Also, effects due to changes in the gap geometry caused by deformations in the gap structure demonstrated that deformations should be considered in the design analysis.

Traineau et al. [10] found that an increase in the angle of attack of 10 to 15 degrees for the same case studied, generated a 48% increase in pressure at the surface and 22% increase in heat transfer. They also showed that increasing the depth and length of the gaps caused a significant increase in temperature. Furthermore, studies have found that three-dimensional effects are important to the size of the vertical flow zone at the top of the gap, where the 3-D size is much smaller than that in 2-D one.

The majority of the available research studies found in the current literature has gone into considering laminar or turbulent flow over a wide range of Mach numbers in the continuum flow regime. Nevertheless, there is little understanding of the physical aspects of hypersonic flow past to gaps related to the severe aerothermodynamic environment associated to a reentry vehicle.

In this scenario, Paolicchi and Santos [12] have studied gaps situated in a rarefied hypersonic flow by employing the DSMC method. The work was motivated by the interest in investigating the length-to-depth (L/H) ratio effect on the flowfield structure. The primary emphasis was to examine the sensitivity of the velocity, density, pressure and temperature due to variations on the gap L/H ratio. It was observed the formation of only one vortex for L/H ratio of 1, 1/2, 1/3 and 1/4. The results showed that the gap flow behavior in the transition flow regime differs from that found in the continuum flow regime for the conditions investigated.

In continuation of the gap study, the present account extends further the previous analysis [12] by investigating the impact of the compressibility on the aerodynamic surface quantities. In this fashion, the primary goal of this paper is to assess the sensitivity of the heat transfer, pressure, and skin friction coefficients due to variations on the freestream Mach number for a family of gaps defined by different L/H ratio. The focus of the present study is the low-density region in the upper atmosphere. At this condition, the degree of molecular non-equilibrium is such that the Navier-Stokes equations are inappropriate. In such a circumstance, the Direct Simulation Monte Carlo (DSMC) method will be employed to calculate the hypersonic two-dimensional flow over the gaps.

2. Computational Tool

In the analysis of aerothermodynamic characteristics of aerospace vehicles, along their descending flight trajectory through the Earth atmosphere, different computational methods are required. At high altitudes, the aerothermodynamic predictions are related to the free molecular or to transition flow regime. In the transition flow regime, the Direct Simulation Monte Carlo (DSMC) method is usually employed. At low altitudes, the aerothermodynamic predictions are related to the continuum flow regime. In this regime, computational methods such as Computational Fluid Dynamics (CFD) are employed. In the present account, the vehicle is subjected to the conditions characterized by the transition flow regime. In this fashion, DSMC method is the suitable computational tool in order to investigate the aerothermodynamic characteristics.

The DSMC method, pioneered by Bird [13], simulates real gas flows with various physical processes by means of a huge number of modeling particles, each of which is a typical representative of a great number of real gas molecules. The reason for that is because it is unfeasible to simulate the real number of particles present in real gases. The state of the modeling particles, position, velocity and internal energy, is stored and modified with time as the particles move, collide, and undergo boundary interactions in the simulated physical space. The simulation is always calculated as unsteady flow. However, the boundary conditions can be applied such that steady flow solution is obtained as the outcome of the large time state of the unsteady flow.

The DSMC method conditionally divides the continuous process of particles movement and collisions into two consecutive stages at each small time step. In the first stage, moving process, all modeling particles are propagated for a time step without collisions. In the second stage, collision process, some randomly chosen pairs of particles in the same cell are allowed to collide and change their velocities without changing their positions. The physical assumption behind this approximation is that the gas is considered as a dilute one. It means that the mean molecular diameter is much smaller than the mean molecular spacing of the gas. In addition, molecular caos is the other assumption behind the method. It means that position and velocities of randomly picked particles are uncorrelated.

Collisions in the present DSMC code are modeled by using the variable hard sphere (VHS) molecular model [14] and the no time counter (NTC) collision sampling technique [15]. Repartition energy among internal and translational modes is controlled by the Larsen-Borgnakke statistical model [16]. Simulations are performed using a non-reacting gas model for a constant freestream gas composition consisting of 76.3% of N_2 and 23.7% of O_2. Energy exchanges between the translational and internal modes, rotational and vibrational, are considered. The probability of an inelastic collision determines the rate at which energy is transferred between the translational and internal modes after an inelastic collision. For a given collision, the probability is defined by the inverse of the number of relaxation, which

corresponds to the number of collisions needed, on average, for a molecule to undergo relaxation. The rates of rotational and vibrational relaxation are dictated by collision numbers Z_R and Z_V, respectively. In the present account, rotational Z_R and vibrational Z_V collision numbers were obtained in a collision energy-based procedure, as suggested by Boyd [17] for rotation and by Bird [18] for vibration.

3. Geometry Definition

In the present account, the gap geometry is the same as that presented in Paolicchi and Santos [12]. It was assumed a flat plate with a gap of length L and depth H. Figure 1 illustrates a schematic view of the model employed. The flat plate was selected by considering that the gap depth H is much smaller than the nose radius R of a reentry vehicle, i.e., $H/R \ll 1$. Therefore, the hypersonic flow over the flat plate with a gap may be representative of the hypersonic flow over a gap located on the surface of a reentry vehicle.

Referring to Fig. 1, M_∞ stands for the freestream Mach number, H is the gap depth, L is the gap length, L_u the length of the gap upstream surface, and L_d the length of the gap downstream surface. It was assumed a length L of 3 mm, and a depth H of 3, 6, 9, and 12 mm. Therefore, the gaps investigated correspond to a length-to-depth ratio, L/H, of 1, 1/2, 1/3 and 1/4, respectively. In addition, L_u/λ_∞ of 50 and L_d/λ_∞ of 50, where λ_∞ is the freestream mean free path. It was considered that the flat plate is infinitely long but only the total length $L_u + L + L_d$ is investigated.

An understanding of the L/H ratio effects on the aerodynamic surface properties can be gained by comparing the flowfield behavior of a flat plate with a gap to that one without a gap. In this manner, a flat plate without a gap works as a benchmark for the cases with a gap, and will be referred herein as the flat-plate case.

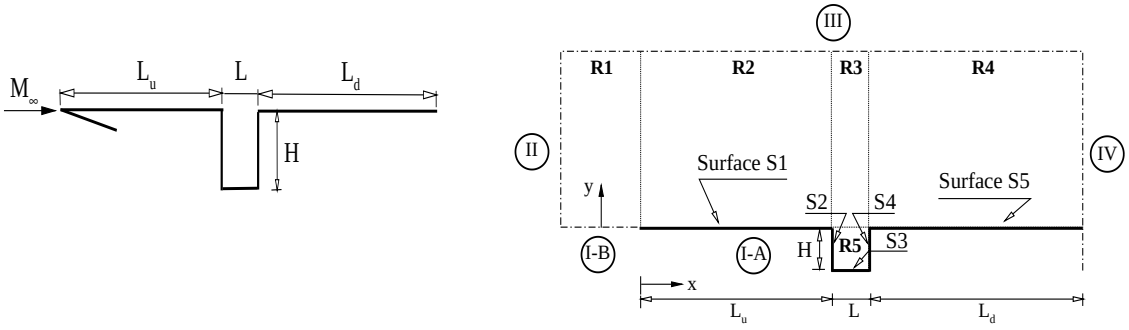

(a) (b)

Figure 1: Drawing illustrating (a) a schematic view of the gap configuration and (b) the computational domain.

4. Freestream and Flow Conditions

Freestream flow conditions used for the numerical simulations are those given by Paolicchi and Santos [12] and summarized in Tab. 1, and the gas properties [13] are shown in Tab. 2. Freestream conditions represent those experienced by a reentry vehicle at an altitude of 70 km.

Table 1: Freestream flow conditions

Altitude (km)	T_∞(K)	p_∞(N/m^2)	ρ_∞(kg/m^3)	n_∞(m^{-3})	λ_∞(m)
70	219.07	5.518	8.752×10^{-5}	1.8193×10^{21}	9.285×10^{-4}

Table 2: Gas properties

	X	m (kg)	d (m)	ω
O_2	0.237	5.312×10^{-26}	4.01×10^{-10}	0.77
N_2	0.763	4.650×10^{-26}	4.11×10^{-10}	0.74

In order to investigate the compressibility effects, the freestream velocity U_∞ is assumed to be constant at 1485.3 m/s, 4527.8 m/s, and 7546.5 m/s, which corresponds to a freestream Mach number M_∞ of 5, 15 and 25, respectively. The translational and vibrational temperatures in the freestream are in equilibrium at 219.07 K. The wall temperature T_w is assumed constant at 880 K. This temperature is chosen to be representative of the surface temperature near the stagnation point of a reentry vehicle and is assumed to be uniform on the gap surface.

The overall Knudsen number Kn is defined as the ratio of the molecular mean free path λ in the freestream gas to a characteristic dimension of the flowfield. In the present study, the characteristic dimension was defined as being the gap depth H. Therefore, the Knudsen number Kn_H corresponds to 0.3095, 0.1548, 0.1032, and 0.0774 for depth H of 3, 6, 9, and 12 mm, respectively. Finally, the Reynolds number Re_H covers approximately from 27 to 487, based on conditions in the undisturbed stream.

5. Computational Flow Domain and Grid

In the DSMC method, the physical space around the body is divided into an arbitrary number of regions, which are subdivided into computational cells. The cells are further subdivided into subcells, usually, two subcells/cell in each coordinate direction. The physical space network is used to facilitate the choice of molecules for collisions and for the sampling of the macroscopic flow properties such as temperature, pressure, etc. In the DSMC algorithm, the linear dimensions of the cells should be small in comparison with the scale length of the macroscopic flow gradients normal to streamwise directions, which means that the cell dimensions should be of the order of or even smaller than the local mean free path [19, 20]. Moreover, the time step should be chosen to be sufficiently small in comparison with the local mean collision time [21, 22].

The computational domain used for the calculation is made large enough so that gap disturbances do not reach the upstream and side boundaries, where freestream conditions are specified. A schematic view of the computational domain is illustrated in Fig. 1(b). According to this figure, side I-A is defined by the gap surface. Diffuse reflection with complete thermal accommodation is the condition applied to this side. Side I-B is a plane of symmetry, where all flow gradients normal to the plane are zero. At the molecular level, this plane is equivalent to a specular reflecting boundary. Sides II and III are the freestream side through which simulated molecules can enter and exit. Side II is positioned at $5\lambda_\infty$ upstream of the flat-plate leading edge, and side III defined at $30\lambda_\infty$ above the flat plate. Finally, the flow at the downstream outflow boundary, side IV, is predominantly supersonic and vacuum condition is specified [13]. As a result, at this boundary, simulated molecules can only exit. It is important to mention that, close to the wall, molecules may not be moving at supersonic speed. Consequently, in this subsonic region close to the wall, there is an interaction between the flow and the downstream boundary. Nevertheless, the extent of the upstream effect of this boundary condition can be determined by changing the length of the gap downstream surface. In doing so, it was found [23] that the upstream disturbance is approximately of $6\lambda_\infty$.

Numerical accuracy in DSMC method depends on the grid resolution chosen as well as on the number of particles per computational cell. Both effects were investigated to determine the number of cells and the number of particles required to achieve grid independence solutions. A grid independence study was made with three different structured meshes – coarse, standard and fine – in each coordinate direction. The effect of altering the cell size in the x-direction was investigated for a coarse and fine grids with, respectively, 50% less and 100% more cells with respect to the standard grid only in the x-direction. Table 3 tabulates the number of cells employed in the five regions (see Fig. 1(b)) for coarse, standard, and fine grids for the $L/H = 1$ case.

In analogous fashion, an examination was made in the y-direction with a coarse and fine grids with, respectively, 50% less and 100% more cells with respect to the standard grid only in the y-direction. In addition, each grid was made up of non-uniform cell spacing in both directions. Moreover, point clustering is used close to solid walls and to the horizontal plane connecting the two corners. The effect (not shown) of changing the cell size in both directions on

Table 3: Number of cells in the (x-direction investigation) and [y-direction investigation] for the $L/H = 1$ case.

	Region 1	**Region 2**	**Region 3**	**Region 4**	**Region 5**	**Total number of cells**
Coarse	(10×80)	(65×110)	(10×110)	(65×120)	(20×40)	17,650
	$[20 \times 40]$	$[130 \times 55]$	$[20 \times 55]$	$[130 \times 60]$	$[40 \times 20]$	17,650
Standard	20×80	130×110	20×110	130×120	40×40	35,300
Fine	(40×80)	(260×110)	(40×110)	(260×120)	(80×40)	70,600
	$[20 \times 160]$	$[130 \times 220]$	$[20 \times 220]$	$[130 \times 240]$	$[40 \times 80]$	70,600

the heat transfer, pressure and skin friction coefficients was rather insensitive to the range of cell spacing considered, indicating that the standard grid, with a total of 35,300 cells, for the $L/H = 1$ case, is essentially grid independent.

A similar examination was made for the number of molecules. The standard grid for the $L/H = 1$ case corresponds to, on average, a total of 741,200 molecules. Two new cases using the same grid were investigated. These two new cases correspond to 370,600 and 1,482,400 molecules in the entire computational domain. As the three cases presented the same results (not shown) for the heat transfer, pressure and skin friction coefficients, hence the standard grid with a total of 741,200 molecules is considered enough for the computation of the flowfield properties. A discussion of the effects of the cell size, time step, and number of molecules variations on the aerodynamic surface quantities for the gaps presented herein is described in detail by Paolicchi [23].

6. Computational Results and Discussion

This section focuses on the effects that take place in the aerodynamic surface quantities due to freestream Mach number variations. Aerodynamic surface quantities of particular interest in the transitional flow regime are number flux, wall pressure, heat flux, and wall shear stress. In this manner, the purpose of this section is to present and to discuss changes in these quantities, expressed in coefficient form, due to variations on the freestream Mach number as well as on the gap L/H ratio.

6.1 Number Flux

The number flux N is calculated by sampling the molecules impinging on the surface by unit time and unit area. The dependence of the number flux along the gap surfaces is illustrated in Figs. 2, 3 and 4 as a function of the freestream Mach number M_∞ and parameterized by the gap L/H ratio. In this group of plots, the dimensionless number flux

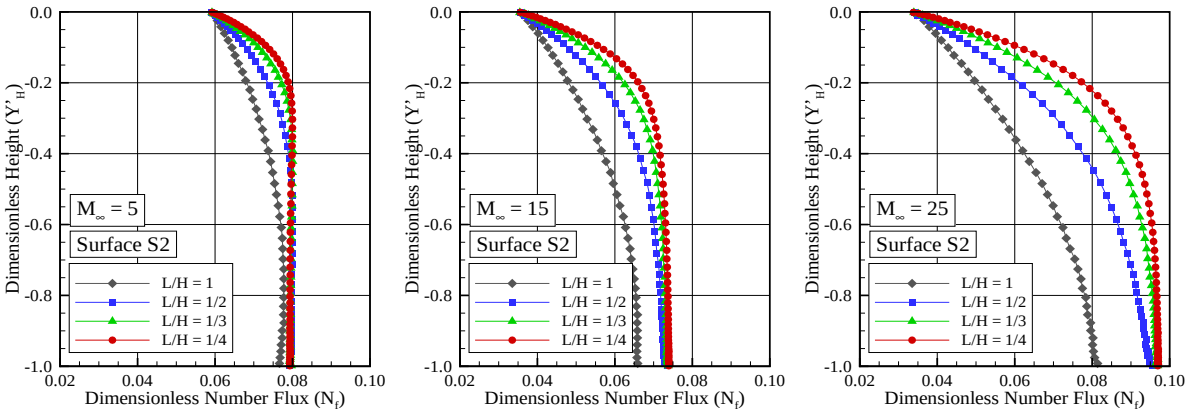

Figure 2: Dimensionless number flux (N_f) distribution along the gap surface $S2$ for M_∞ of (a) 5, (b) 15, and (c) 25.

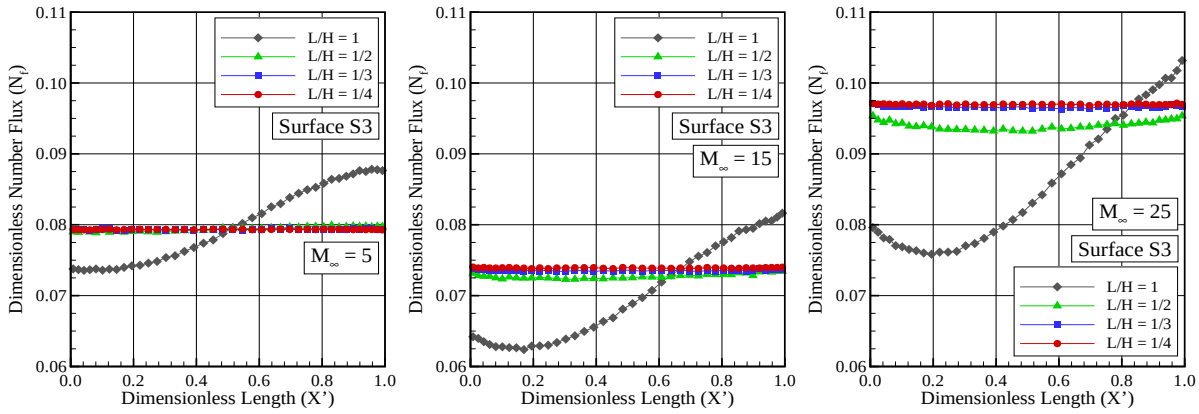

Figure 3: Dimensionless number flux (N_f) distribution along the gap surface $S3$ for M_∞ of (a) 5, (b) 15, and (c) 25.

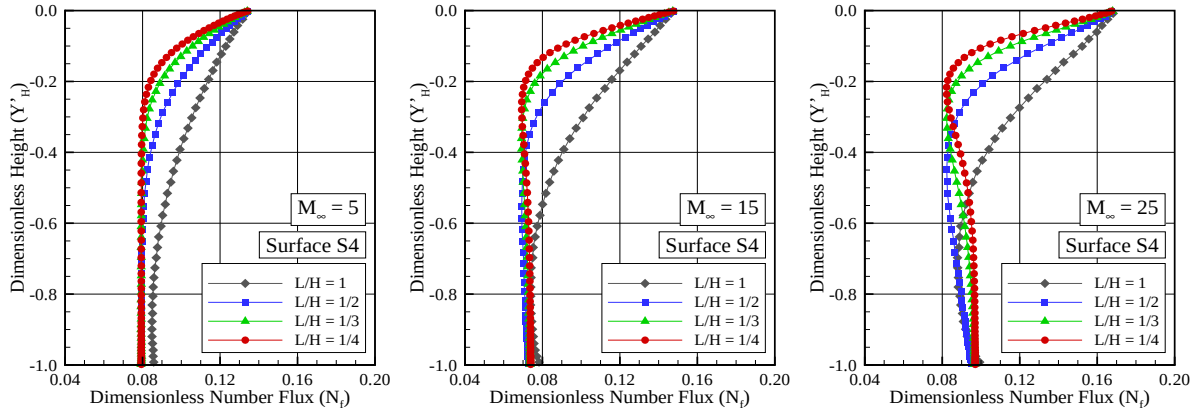

Figure 4: Dimensionless number flux (N_f) distribution along the gap surface $S4$ for M_∞ of (a) 5, (b) 15, and (c) 25.

N_f represents the number flux N normalized by $n_\infty U_\infty$, where n_∞ is the freestream number density and U_∞ is the freestream velocity. It is important to recall that U_∞ differs for each Mach number case investigated. In addition, the dimensionless height Y'_H is the height y normalized by the gap depth H, and X' represents the distance $(x - L_u)$ normalized by the gap length L. Also, $S2$ and $S4$ stand for the upstream and downstream gap faces, and $S3$ for the bottom gap surface or gap floor, as defined in Fig. 1(b).

Looking first at Figs. 2(a-c), it is seen that the dimensionless number flux N_f to the upstream surface relies on the gap L/H ratio and on the freestream Mach number M_∞. The dimensionless number flux N_f is low at the top of the gap, $Y'_H = 0$, and increases monotonically along the surface $S2$ up to the corner at the bottom surface, $Y'_H = -1.0$, where N_f reaches the peak values. Particular attention is paid to the number flux for freestream Mach number of 15, Fig. 2(b). It is clearly noticed that, for the $M_\infty = 15$ case, N_f is smaller than that for the $M_\infty = 5$ case. The reason for that is because the number flux N is normalized by the amount $n_\infty U_\infty$. Even though N_f slightly decreased for the $M_\infty = 15$ case, the number flux N increases as the freestream Mach number increases from 5 to 25.

According to Figs. 3(a-c), along the gap floor, surface S3, the number flux behavior also relies on the L/H ratio as well as on the freestream Mach number. It is observed that, in general, N_f increases with decreasing the L/H ratio. Nevertheless, it is seen that N_f reaches a constant value for $L/H < 1/3$. It is also observed that the number flux N increases with increasing the freestream Mach number from 5 to 25.

Turning next to Figs. 4(a-c), along the downstream face, surface S4, N_f basically increases from the corner, at

the bottom surface, $Y'_H = -1.0$, up to the top of the gap, $Y'_H = 0.0$. This behavior is in contrast to that observed for the upstream face, surface $S2$. In fact, this is an expected behavior in the sense that it is directly related to the flow recirculation that appears inside the gap [23]. Due to the clockwise flow recirculation, at the vicinity of the surface S4, density is higher than that close to the surface S2. Therefore, a large flux of molecules colliding to this surface is expected.

6.2 Heat Transfer Coefficient

The heat transfer coefficient C_h is defined as follows,

$$C_h = \frac{q_w}{\frac{1}{2}\rho_\infty U_\infty^3} \tag{1}$$

where the heat flux q_w to the body surface is calculated by the net energy flux of the molecules impinging on the surface. A flux is regarded as positive if it is directed toward the body surface. The net heat flux q_w is related to the sum of the translational, rotational and vibrational energies of both incident and reflected molecules as defined by,

$$q_w = q_i - q_r = \frac{F_N}{A\Delta t}\{\sum_{j=1}^{N}[\frac{1}{2}m_j c_j^2 + e_{Rj} + e_{Vj}]_i - \sum_{j=1}^{N}[\frac{1}{2}m_j c_j^2 + e_{Rj} + e_{Vj}]_r\} \tag{2}$$

where F_N is the number of real molecules represented by a single simulated molecule, Δt is the time step, A the area, N is the number of molecules colliding with the surface by unit time and unit area, m is the mass of the molecules, c is the velocity of the molecules, e_R and e_V stand for rotational and vibrational energies, respectively. Subscripts i and r refer to incident and reflect molecules.

The impact of the freestream Mach number on the heat transfer coefficient C_h to the gap surfaces, $S2$, $S3$, and $S4$, is demonstrated in Figs. 5, 6 and 7, respectively, as a function of the gap L/H ratio.

According to Figs. 5(a-c), it is noticed that, except to the $M_\infty = 5$ case, the heat transfer coefficient is high at the top of the gap and slightly increases to a maximum value still close to the shoulder, surface-S1/surface-S2 junction. Afterwards, C_h drops off along the surface $S2$ up to the corner at the bottom surface, surface $S3$. Along the gap floor, Figs. 6(a-c), the heat transfer coefficient C_h depends on the L/H ratio. It is noted that the behavior for the $L/H = 1$ case differs from those cases defined by $L/H < 1$. While C_h increases up to a peak value close to the surface-S3/surface-S4 junction for the $L/H = 1$ case, C_h practically goes to zero for the cases defined by $L/H < 1$. It should be remarked in this context that, for $L/H < 1$ cases, the recirculation region does not reach the bottom of the gaps, as shown by Paolicchi [23]. Also, density is higher in this region. As a result, the molecular collision rate is larger compared to the other regions, and the flow comes to the thermal equilibrium and reaches the prescribed wall temperature [23].

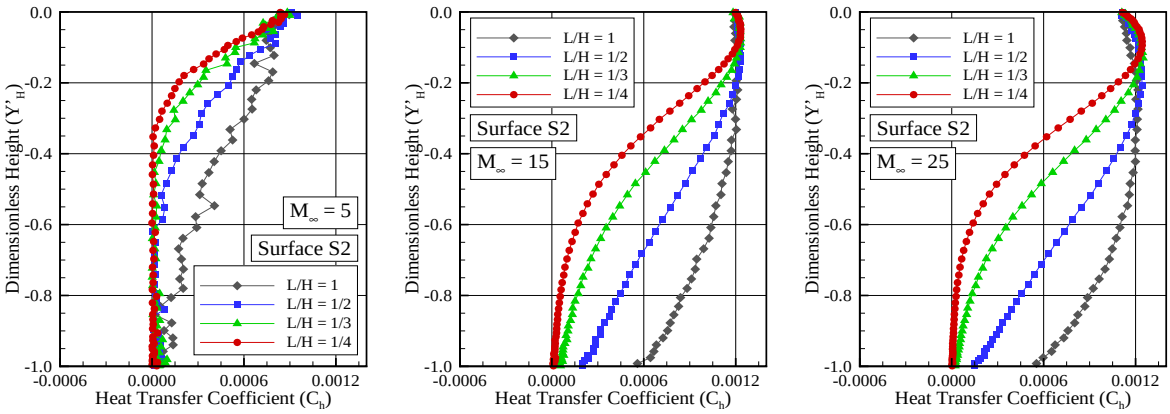

Figure 5: Heat transfer coefficient (C_h) distribution along the gap surface $S2$ for M_∞ of (a) 5, (b) 15, and (c) 25.

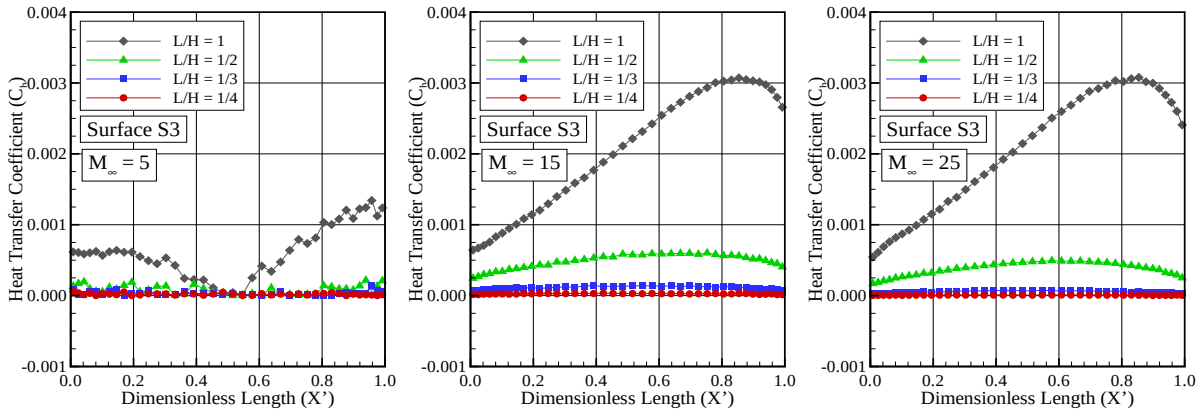

Figure 6: Heat transfer coefficient (C_h) distribution along the gap surface $S3$ for M_∞ of (a) 5, (b) 15, and (c) 25.

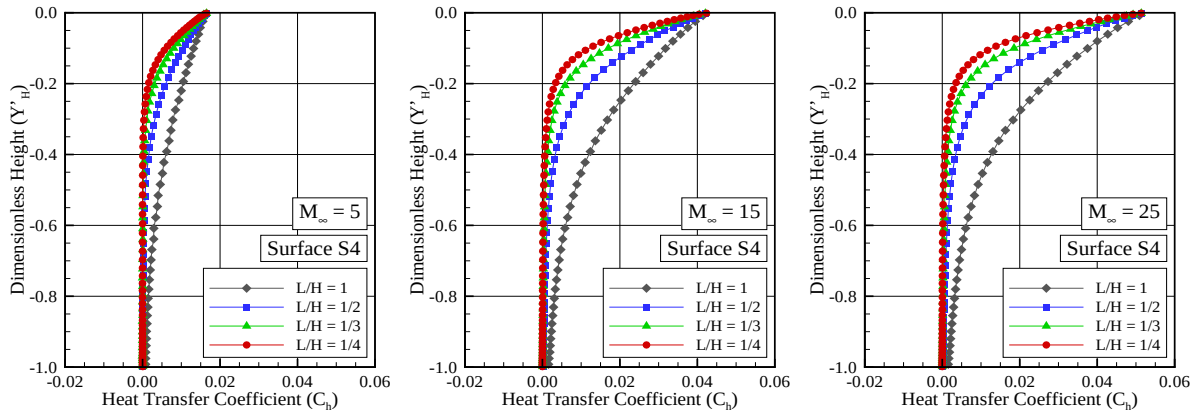

Figure 7: Heat transfer coefficient (C_h) distribution along the gap surface $S4$ for M_∞ of (a) 5, (b) 15, and (c) 25.

Referring to Figs. 7(a-c), along the downstream face, surface S4, the heat transfer coefficient C_h increases monotonically from basically zero, at the surface-S3/surface-S4 junction, to a maximum value that take place at the vicinity of the surface-S4/surface-S5 junction. It is also observed that this maximum value increases with increasing the freestream Mach number, for the cases investigated in the present account. As a base of comparison, peak values for C_h are around to 0.016, 0.042, and 0.051 for freestream Mach number M_∞ of 5, 15, and 25, respectively. As indeed is clear from these plots, these peak values are basically independent of the L/H ratio. For completeness, according to Paolicchi [23], the heat transfer coefficient C_h for a flat plate without a gap, based on the same freestream conditions, with freestream Mach number of 25, the maximum value for C_h is around to 0.030 at a station $8.6\lambda_\infty$ from the leading edge. Therefore, the peak value of C_h for the gap is almost twice of that for a smooth surface.

It is very encouraging to observe that the heat transfer coefficient C_h for the downstream face, surface $S4$, is roughly one order of magnitude larger than that for the bottom surface, and this is one order of magnitude larger than that for the upstream face, surface $S2$. The reason for that is because at the vicinity of the upstream face the flow experiences a expansion. In contrast, at the vicinity of the downstream face, it experiences a compression due to the recirculation structure inside the gaps [23].

The heat flux to the body surface was defined in terms of the incident and reflected flow properties, Eq.(2), and based upon the gas-surface interaction model of fully accommodated, complete diffuse re-emission. The diffuse model assumes that the molecules are reflected equally in all directions, quite independently of their incident speed and direction. Due to the diffuse reflection model, the reflected velocity of the molecules impinging on the body surface is

obtained from a Maxwellian distribution that takes into account for the temperature of the body surface. In this fashion, according to Eq.(2), not only the number of molecules impinging on the surface but also the wall temperature plays a important role on the reflected contribution to the net heat flux to the body surface.

6.3 Pressure Coefficient

The pressure coefficient C_p is defined as follows,

$$C_p = \frac{p_w - p_\infty}{\frac{1}{2}\rho_\infty U_\infty^2} = \frac{p_w/p_\infty - 1}{\frac{1}{2}\gamma M_\infty^2} \tag{3}$$

where p_∞ is the freestream pressure, γ is the specific heat ratio, and the pressure p_w on the body surface is calculated by the sum of the normal momentum fluxes of both incident and reflected molecules at each time step as follows,

$$p_w = p_i - p_r = \frac{F_N}{A\Delta t}\sum_{j=1}^{N}\{[(mv)_j]_i - [(mv)_j]_r\} \tag{4}$$

where v is the velocity component of the molecule j in the surface normal direction.

The effect on pressure coefficient C_p due to variations on the freestream Mach number M_∞ and on the L/H ratio is demonstrated in Figs. 8, 9, and 10 for gap surfaces $S2$, $S3$, and $S4$, respectively.

According to Figs. 8(a-c), which correspond to the upstream face, surface $S2$, it is seen that the pressure coefficient C_p basically follows the same trend as that presented by the number flux in the sense that it is low at the shoulder, station $Y'_H = 0$, and increases downward along the surface, reaching the maximum value at the bottom, $Y'_H = -1.0$. In the following, referring to Figs. 9(a-c), along the gap floor, surface $S3$, the pressure coefficient for the $L/H = 1$ case increases along the entire surface, and reaches the maximum value at the vicinity of the surface-$S3$/surface-$S4$ junction. In contrast, for the $L/H < 1$, the pressure coefficient is constant along the entire surface. Finally, based on Figs. 10(a-c), along the downstream face, surface $S4$, the pressure coefficient behavior is in contrast to that observed along the surface $S2$ in the sense that C_p presents the lower value at the station $Y'_H = -1.0$, and increases monotonically upward along the surface, reaching the peak value at the shoulder, $Y'_H = 0$. It should be mentioned in this context that this is an expected behavior since the flow within the gaps is characterized by the appearance of a recirculation region. According to Paolicchi [23], the streamline pattern showed that the flow is characterized by a primary vortex system for the L/H ratio investigated, where a clockwise recirculating structure filled the entire gap for the $L/H = 1$. Conversely, for the $L/H < 1$ cases, the flow was still characterized by a primary vortex, nevertheless, the recirculation did not fill the whole gaps.

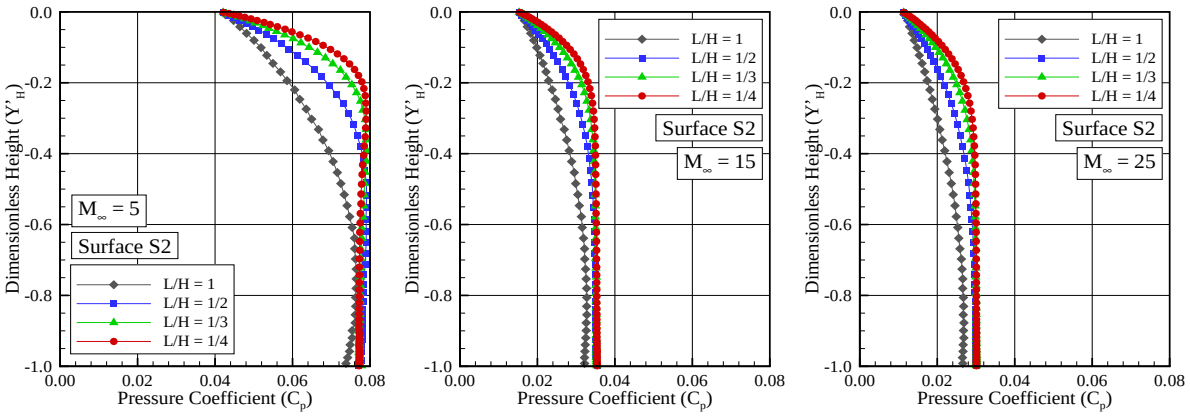

Figure 8: Pressure coefficient (C_p) distribution along the gap surface $S2$ for M_∞ of (a) 5, (b) 15, and (c) 25.

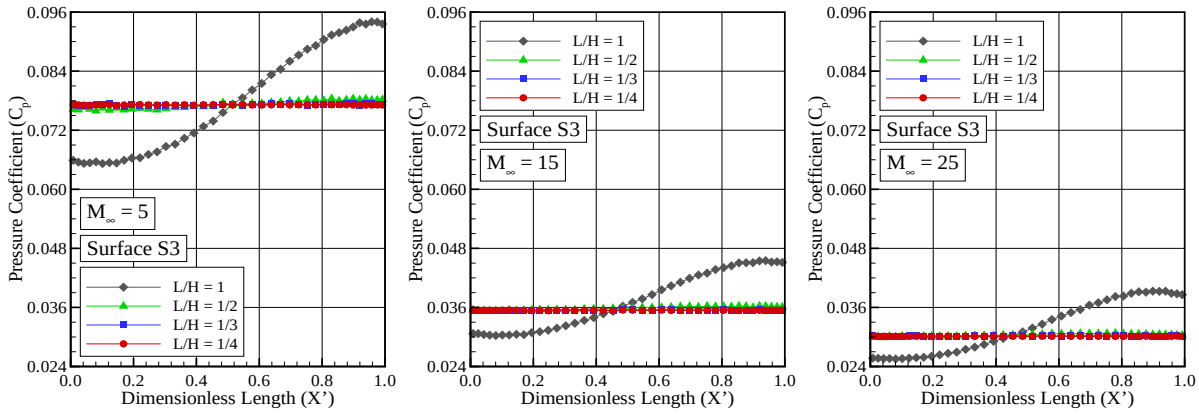

Figure 9: Pressure coefficient (C_p) distribution along the gap surface $S3$ for M_∞ of (a) 5, (b) 15, and (c) 25.

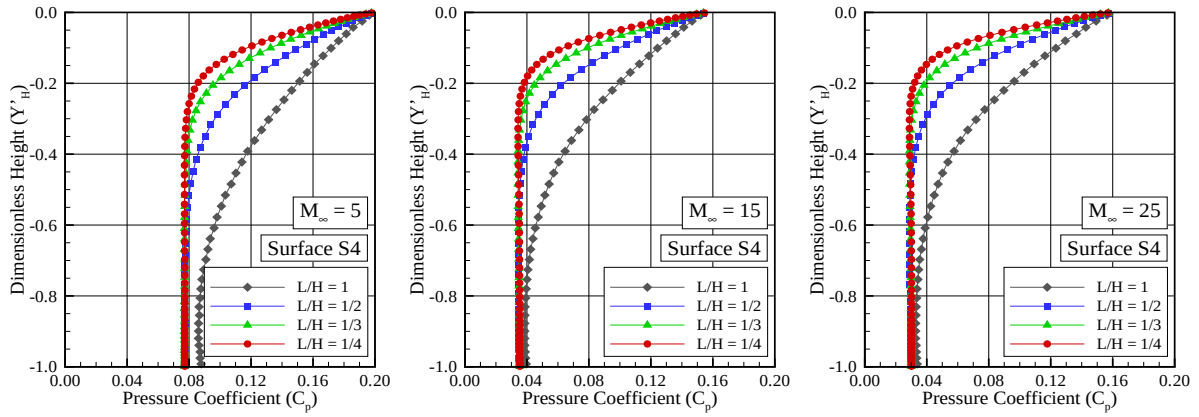

Figure 10: Pressure coefficient (C_p) distribution along the gap surface $S4$ for M_∞ of (a) 5, (b) 15, and (c) 25.

It may be recognized from Figs. 8, 9, and 10 that the freestream Mach number rise contributed to decrease the pressure coefficient along the surfaces $S2$, $S3$ and $S4$, for the freestream Mach number range investigated. However, it is very encouraging to observe that, although the pressure coefficient C_p is decreasing with the freestream Mach number rise, the wall pressure p_w is increasing with increasing the freestream Mach number. An understanding of this behavior can be gained by analyzing Eq. (3). According to this equation, C_p is inversely proportional to the freestream Mach number. Therefore, even though the numerator (p_w) of Eq. (3) increases with increasing M_∞, the denominator increases with M_∞^2. As a result, a reduction in the pressure coefficient C_p is observed for the freestream Mach number range investigated.

In the following, it proves helpful to compare the maximum values for the pressure coefficient observed in the gaps with that of a smooth surface, i.e., a flat plate without a gap. As a basis of comparison, the peak values for C_p is around 0.157, 0.154, and 0.157 for M_∞ of 5, 15 and 25, respectively, observed at the gap shoulder, surface $S4$. According to Paolicchi [23], for the same flow conditions with a freestream Mach number of 25, the maximum value for C_p is around to 0.047 at a station $28.3\lambda_\infty$ from the leading edge. Therefore, the peak value of C_p for the gap is around three times larger than that for a smooth surface.

6.4 Skin Friction Coefficient

The skin friction coefficient C_f is defined as follows,

$$C_f = \frac{\tau_w}{\frac{1}{2}\rho_\infty U_\infty^2} = \frac{\tau_w/p_\infty - 1}{\frac{1}{2}\gamma M_\infty^2} \tag{5}$$

where the shear stress τ_w on the body surface is calculated by the sum of the tangential momentum fluxes of both incident and reflected molecules impinging on the surface at each time step by the following expression,

$$\tau_w = \tau_i - \tau_r = \frac{F_N}{A\Delta t}\sum_{j=1}^{N}\{[(mu)_j]_i - [(mu)_j]_r\} \tag{6}$$

where u is the velocity component of the molecule j in the surface tangential direction.

It is worthwhile to note that for the special case of a diffuse reflection, the gas-surface interaction model adopted herein, the reflected molecules have a tangential moment equal to zero, since the molecules essentially lose, on average, their tangential velocity components. In this manner, the net tangential momentum flux is defined as follows,

$$\tau_w = \tau_i = \frac{F_N}{A\Delta t}\sum_{j=1}^{N}\{[(mu)_j]_i\} \tag{7}$$

The impact of the freestream Mach number on the skin friction coefficient C_f is depicted in Figs. 11, 12, and 13 for gap surfaces $S2$, $S3$, and $S4$, respectively. According to Figs. 11(a-c), for the upstream face, surface $S2$, it is noticed that the skin friction coefficient in general presents the peak value at the shoulder, $Y'_H = 0$, decreases downward along the surface up to the surface-$S2$/surface-$S3$ junction. For the particular case of $L/H = 1$, C_f becomes negative from station $Y'_H \approx$ -0.8 up to $Y'_H = 0.0$. In what follows, referring to Figs. 12(a-c), for the gap floor, surface $S3$, the skin friction coefficient behavior relies on the L/H ratio. It is negative near the vicinity of the surface-$S2$/surface-$S3$ junction, then it becomes positive and reaches a maximum value as a function of the L/H ratio. Finally, based on Figs. 13(a-c), along the downstream face, surface $S4$, the skin friction coefficient C_f increases negatively upward along the entire surface. Usually, as C_f changes from positive to negative value, the condition $C_f = 0$ may indicate the presence of a backflow, an attachment or reattachment point in the flow. In the present account, these changes are directly related to the clockwise recirculation structure, defined by a primary vortex system observed for the gap L/H ratio investigated.

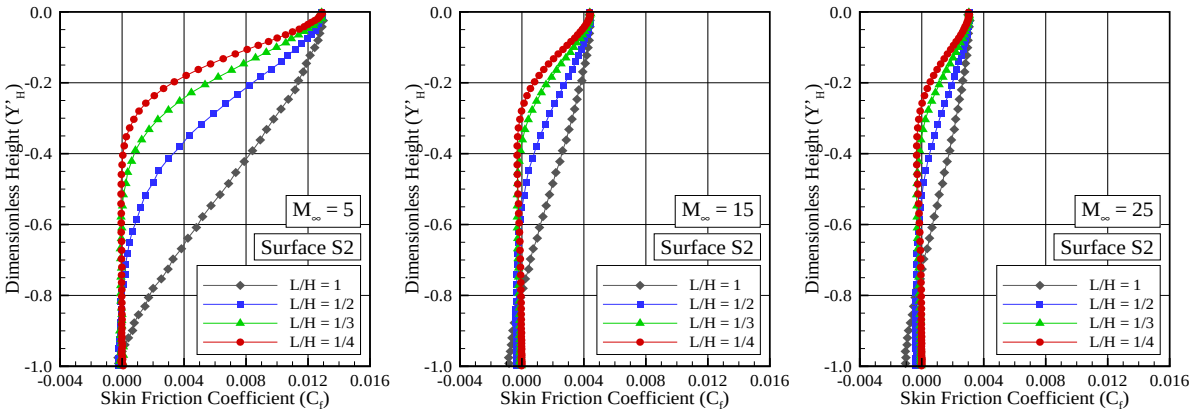

Figure 11: Skin friction coefficient (C_f) distribution along the gap surface $S2$ for M_∞ of (a) 5, (b) 15, and (c) 25.

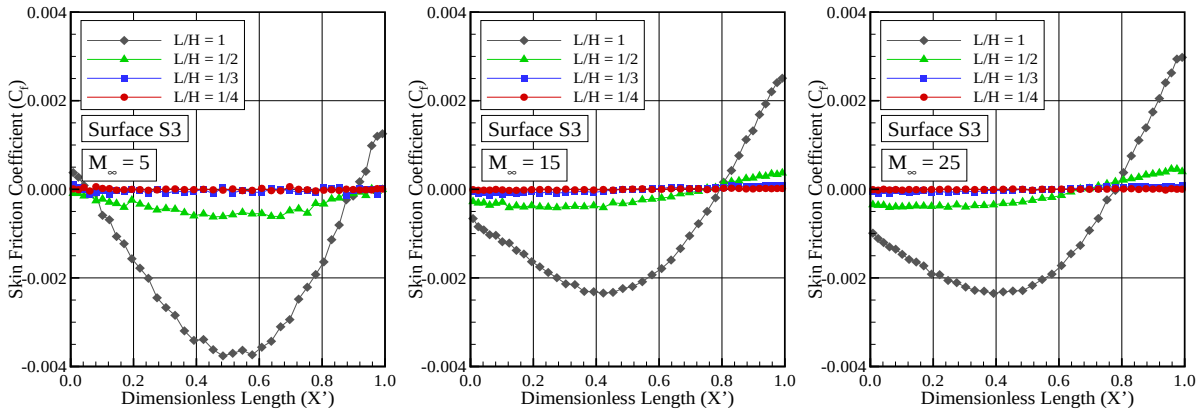

Figure 12: Skin friction coefficient (C_f) distribution along the gap surface $S3$ for M_∞ of (a) 5, (b) 15, and (c) 25.

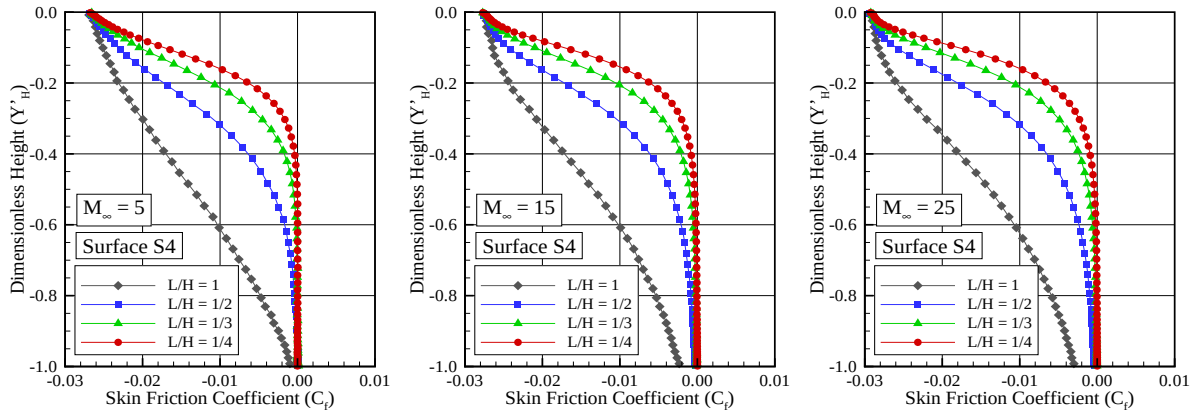

Figure 13: Skin friction coefficient (C_f) distribution along the gap surface $S4$ for M_∞ of (a) 5, (b) 15, and (c) 25.

It is quite apparent from Figs. 11, 12, and 13 that the freestream Mach number rise contributed to decrease the skin friction coefficient along the surfaces $S2$, $S3$ and $S4$, for the freestream Mach number range investigated. Again, similar to the behavior for the pressure coefficient C_p, is noteworthy that, although the skin friction coefficient C_f is decreasing with the freestream Mach number rise, the wall shear stress τ_w is increasing with increasing the freestream Mach number. According to Eq. (5), C_f is inversely proportional to the freestream Mach number. Therefore, even though the numerator (τ_w) of Eq. (5) increases with increasing M_∞, the denominator increases with M_∞^2. Consequently, a reduction in the skin friction coefficient C_f is observed for the freestream Mach number range investigated.

7. Concluding Remarks

Computations of a rarefied hypersonic flow on a family of gaps have been performed by using the Direct Simulation Monte Carlo (DSMC) method. The calculations provided information concerning the nature of the aerodynamic surface quantities on the gap surfaces. Effects of the freestream Mach number and of the length-to-depth ratio on the number flux, heat transfer, pressure and skin friction coefficients for a representative range of parameters were investigated. The freestream Mach number varied from 5 to 25, and the length-to-depth ratio ranged from 1 to 1/4, which corresponded Knudsen numbers in the transitional flow regime.

On the basis of the foregoing results it can be concluded that, for the range of the conditions investigated in

the present study, the aerodynamic quantities acting on the gap surface depended on the L/H ratio. In contrast, the aerodynamic surface quantities did not presented a significant dependence on the freestream Mach number. It was found that the pressure load and the heat load presented the maximum values along the downstream face at the shoulder of the gaps. In addition, these loads are much larger than those attained in a smooth surface.

8. Acknowledgements

The authors would like to thank the financial support provided by CNPq (Conselho Nacional de Desenvolvimento Científico e Tecnológico) under Grant No. 473267/2008-0.

References

[1] Dunavant, J. C., and Throchmorton, D. A., 1974. Aerodynamic heat transfer to RSI tile surfaces and gap intersections. *Journal of Spacecraft and Rockets*, 11:437–440.

[2] Scott, C. D., and Maraia, R. J., 1979. Gap heating with pressure gradients. In:*14th AIAA Thermophysics Conference*, AIAA Paper 79–1043, Orlando, FL, USA.

[3] Bertin, J. J., and Goodrich, W. D., 1980. Aerodynamic heating for gaps in laminar and trasitional boundary layers. In: *18th AIAA Aerospace Sciences Meeting and Exhibit*, AIAA Paper 80–0287, Pasadena, CA, USA.

[4] Pitts, W. C., and Murbach, M. S., 1982. Flight measurements of tile gap heating on the space shuttle. In: *AIAA/ASME 3rd Joint Thermophysics, Fluids, Plasma and Heat Transfer Conference*, AIAA Paper 82–0840, St. Louis, MO, USA.

[5] Smith, D. M., Petley, D. N., Edwards, C. L. W., and Patten, A. B., 1983. An investigation of gap heating due to stepped tiles in zero pressure gradient regions of the shuttle orbiter thermal protection system. In: *21st AIAA Aerospace Sciences Meeting and Exhibit*, AIAA Paper 83-0120, Reno, NV, USA.

[6] Petley, D. H., Smith, D. M., Edwards, C. L. W., Carlson, A. B., and Hamilton II, H. H., 1984. Surface step induced gap heating in the shuttle thermal protection system. *Journal of Spacecraft and Rockets*, 11:156–161.

[7] Higdon, J. J. L., 1985. Stokes flow in arbitrary two-dimensional domains: shear flow over ridges and cavities. *Journal of Fluid Mechanics*, 159:195–226.

[8] Charbonnier, J., and Boerrigter, H., 1993. Contribution to the study of gap induced boundary layer transition in hypersonic flow. In: *AIAA/DGLR 5th International Aerospace Planes and Hypersonics Technologies Conference*, AIAA Paper 93–5111, Munich, Germany.

[9] Hinderks, M., Radespiel, R., and Gülhan, A., 2004. Simulation of hypersonic gap flow with consideration of fluid structure interaction. In: *34th AIAA Fluid Dynamics Conference and Exhibit*, AIAA Paper 2004–2238, Portland, OR, USA.

[10] Traineau, J. C., Thivet, F., Gulhan, A., Cosson, E., Smith, A., and Marraffa, L., 2005. Synthesis of the gap heating analysis of the hyflex flight. In: *Proceedings of the Fifth European Symposium on Aerothermodynamics for Space Vehicles*.

[11] Hinderks, M., and Radespiel, R., 2006. Investigation of hypersonic gap flow of a reentry nosecap with consideration of fluid structure interaction. In: *44th AIAA Aerospace Sciences Meeting and Exhibit*, AIAA Paper 2006-0188, Reno, NV, USA.

[12] Paolicchi, L. T. L. C., and Santos, W. F. N., 2009. Direct simulation calculations of rarefied hypersonic gap flow. In: *3rd Southern Conference on Computational Modeling*, Rio Grande, RS, Brazil.

[13] Bird, G. A., 1994. *Molecular gas dynamics and the direct simulation of gas flows*, Oxford University Press.

[14] Bird, G. A., 1981. Monte Carlo simulation in an engineering context. In: *Progress in Astronautics and Aeronautics: Rarefied gas Dynamics*, AIAA New York, 74:239–255.

[15] Bird, G. A., 1989. Perception of numerical method in rarefied gasdynamics. In: *Rarefied Gas Dynamics: Theoretical and Computational Techniques*, Progress in Astronautics and Aeronautics, AIAA, New York, 118:374–395.

[16] Borgnakke, C. and Larsen, P. S., 1975. Statistical collision model for Monte Carlo simulation of polyatomic gas mixture. *Journal of Computational Physics*, 18:405–420.

[17] Boyd, I. D., 1998. Analysis of rotational nonequilibrium in standing shock waves of nitrogen. *AIAA Journal*, 28:1997–1999.

[18] Bird, G. A., 2009. A Comparison of collision energy-based and temperature-based procedures in DSMC. In: *Rarefied Gas Dynamics: 26th International Symposium*, American Institute of Physics, 245–250.

[19] Alexander, F. J., Garcia, A. L., and Alder, B. J., 1998. Cell size dependence of transport coefficient in stochastic particle algorithms. *Physics of Fluids*, 10:1540–1542.

[20] Alexander, F. J., Garcia, A. L., and Alder, B. J., 2000. Erratum: cell size dependence of transport coefficient in stochastic particle algorithms. *Physics of Fluids*, 12:731–731.

[21] Garcia, A. L., and Wagner, W., 2000. Time step truncation error in direct simulation Monte Carlo. *Physics of Fluids*, 12:2621–2633.

[22] Hadjiconstantinou, N. G., 2000. Analysis of discretization in the direct simulation Monte Carlo. *Physics of Fluids*, 12:2634–2638.

[23] Paolicchi, L. T. L. C., 2010. Computational analysis of gap effects on the surface of reentry apace vehicles. MS Thesis, National Institute for Space Research (INPE), Combustion and Propulsion Laboratory.